ACS Catalysis

Research Article

pubs.acs.org/acscatalysis

Composite Electrode Boosts the Activity of $Ba_{0.5}Sr_{0.5}Co_{0.8}Fe_{0.2}O_{3-\delta}$ Perovskite and Carbon toward Oxygen Reduction in Alkaline Media

Emiliana Fabbri,*[,†] Rhiyaad Mohamed,[‡] Pieter Levecque,[‡] Olaf Conrad,[‡] Rüdiger Kötz,[†] and Thomas J. Schmidt[†]

[†]Electrochemistry Laboratory, Paul Scherrer Institut, 5232 Villigen, Switzerland

[‡]HySA/Catalysis Centre of Competence, Centre for Catalysis Research, Department of Chemical Engineering, University of Cape Town, Rondebosch 7701, South Africa

Supporting Information

ABSTRACT: Herein we report the electrochemical activity and selectivity toward the oxygen reduction reaction (ORR) for composite electrodes made of $Ba_{0.5}Sr_{0.5}Co_{0.8}Fe_{0.2}O_{3-\delta}$ (BSCF) perovskite oxide and Acetylene black (AB) carbon in alkaline media. The onset potential and the selectivity, i.e., hydroperoxide formation, toward the ORR exhibit a volcano type behavior as a function of the electrode composition. The HO_2^- formation measured by rotating ring disk electrode technique decreases from about 60% and 70% for the BSCF and the AB, respectively, to 28% for the electrode having a BSCF/AB weight ratio of 1.25 (values taken at 0.4 V vs RHE). Accordingly, the value for the overall transferred electrons is significantly larger (around 3.5) for the composite electrode compared to individual materials. Therefore, the overall results point toward a beneficial interaction between BSCF and AB. Different scenarios are considered; first an improved electrical connection of BSCF particle agglomerates upon carbon addition. However, the latter cannot fully explain the significant improvement in ORR activity and selectivity for the composite electrodes. By measuring the BSCF electrochemical activity toward HO_2^- reduction, we can exclude the occurrence of a synergistic ORR process where oxygen is first reduced on AB to OH_2^-, and then further electroreduced to OH^- by the BSCF. Besides the activity toward hydroperoxide electroreduction, the potential of BSCF as catalyst for the hydroperoxide disproportionation reaction is also investigated, and even though a certain catalytic activity exists, the perovskite oxide shows rather low decomposition rate. These results might suggest that ligand (electronic) effects between the two materials also play a role in the enhanced ORR activity of the composite electrodes.

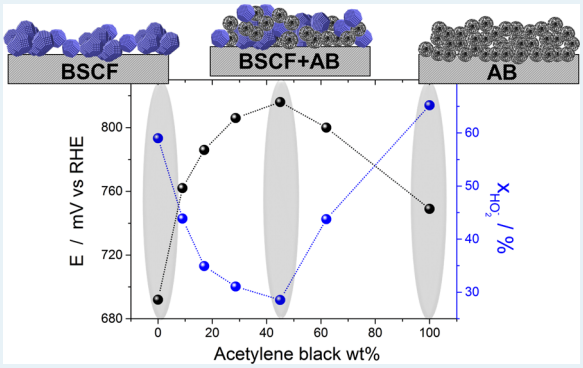

KEYWORDS: *Energy conversion, oxygen electrocatalysis, fuel cells, cathode materials, non-noble metal catalysts, oxides*

INTRODUCTION

Alkaline fuel cells (AFCs) were the first mature low temperature fuel cell technology developed in the 1960s and mainly used for space program applications.[1] However, mostly due to the electrolyte deterioration when in contact with CO_2, the interest in these systems has been shelved for many years. In the past decade, the field has been rejuvenated due to the development of CO_2 rejecting alkaline OH^- conducting membranes[2] and many further developments have been undertaken in both academic and industrial environments. Besides ohmic contributions, in AFCs (or alkaline membrane fuel cells, AMFCs), the main voltage loss is due to the slow kinetics of the positive electrode where the oxygen reduction reaction (ORR) takes place. Platinum represents a stable and highly active electrocatalyst for the ORR, but as most of the noble metals it is a rather limited and expensive resource. Compared to low temperature fuel cell systems based on acidic electrolytes, AFCs allow for the investigation of a wider range of catalyst materials due to the higher stability of a broad range of metals, alloys and even oxides, offering favorable oxygen electrocatalysis in the alkaline environment.[3] Therefore, several materials have been intensively investigated as alternative ORR catalysts to noble metals for application in AFCs or alkaline-based energy conversion devices. Materials of interest for such applications include carbons,[4] various transition metals,[5] metal macrocycles[6] and metal oxides.[7−9] Particularly, one class of metal oxides that has shown the potential of high electrocatalytic activity is perovskites. This type of oxide has the general formula ABO_3 where the A site is occupied by an alkaline earth element, such as Ba, Sr or Ca, and the B site is occupied by a transition metal element in 6-fold coordination to the oxygen atoms. The ABO_3 structure can accommodate

Received: October 10, 2013
Revised: February 6, 2014
Published: February 21, 2014

cation substitution in a wide range by partial substitution of either the A and/or B cation with another element giving $(A_xA'_{1-x})(B_yB'_{1-y})O_3$ compositions. Such substitutions lead to modification of the perovskite band structure and also to creation of oxygen vacancies, determining the electrical, optical and magnetic properties of these materials and, thus, may also significantly influence their catalytic activity.

The potential of perovskites as oxygen electrocatalysts in alkaline media has been known since the early 1970s when a variety of bulk physical properties, such as band structure, was examined and correlated with the catalytic activity of these compounds.[10−13] Recently, the attention has been once more pointed toward a correlation between band structure and perovskite catalytic activity.[14,15] In particular, it was found out that the highest activity toward oxygen electrocatalysis (reduction and evolution) can be achieved for perovskites presenting e_g orbital occupancy close to unity. $Ba_{0.5}Sr_{0.5}Co_{0.8}Fe_{0.2}O_{3-\delta}$ (BSCF), which fulfills this criteria, has shown the highest catalytic activity toward the oxygen evolution reaction.[15] Because the same band descriptor has been reported to be effective in designing superior ORR catalysts as well,[14] the band structure configuration of BSCF therefore suggests that this material should exhibit promising ORR catalytic activity as well. In a previous work[16] we have thus investigated the ORR activity and mechanism of BSCF powder in alkaline environment. The onset for the ORR on the BSCF surface occurs at rather high overpotential and the reaction does not lead to 4-electron exchange, but rather results in parallel OH^- and HO_2^- formation that it does not fit into the volcano curves presented in ref 14. Given the poor performance of BSCF as a single electrode component, in the present work, composite electrodes made of BSCF and carbon have been designed and investigated in order to boost the ORR catalytic activity.

Most of the recent studies on perovskite ORR activity in alkaline media utilize carbon as a second electrode component with the aim of eliminating any possible concern about perovskite particle electronic connection.[14,15,17−21] Different carbons such as high surface area Vulcan XC 72[17,22] or Ketjen black,[18] and lower surface area Acetylene black[14,19,23] or Super P[20] carbons have been used in combination with perovskite catalysts, generally in an oxide to carbon weight ratio range between 5:1 and 1:1. However, even carbons with relative low surface area, such as Acetylene black or Super P, possess a significantly higher BET surface area compared to that of perovskite powders and remarkable activity toward ORR in alkaline media.[4] If we consider a low surface area carbon such as Acetylene black (about 80−100 $m^2\ g^{-1}$) and a perovskite oxide with an average surface area of about 10 $m^2\ g^{-1}$ (among those reported in the literature[14,15,17,19−25]), a given oxide to carbon weight ratio of 5:1 would mean a surface area ratio of about 1:2. This easy calculation indicates that the addition of only 20 wt % of carbon into the electrodes would result in double the carbon surface area compared to that of the perovskite catalyst. Given that the ORR is a purely surface electrochemical process and taking into account the non-negligible carbon ORR activity in alkaline media, a catalyst electrode comprising of perovskite and carbon in a 5:1 weight ratio should definitively be considered as a composite electrode. These arguments point out the critical importance of understanding the role of carbon itself and its effect on the perovskite catalysts in catalyzing the ORR, i.e., whether the carbon in perovskite/carbon composite electrodes plays only a simple role of conductive support or if its introduction as second electrode component influences the ORR mechanistic pathways. Synergistic effects between binary oxides and carbon toward the ORR in alkaline media have been reported in literature, leading to composite oxide/carbon catalysts with excellent performance toward the ORR.[8,9,26] Recent publications on perovskite catalysts[22−24,27] have provided evidence of synergistic effects between some perovskite oxides and carbon toward ORR in alkaline media. Therefore, in this paper, we demonstrate the activity boost of BSCF toward the ORR and unravel possible synergetic interaction between BSCF and carbon. Several composite electrodes were systematically investigated by varying the ratio between BSCF and Acetylene black carbon. Furthermore, the ORR activity and hydroperoxide formation of a single electrode component made of BSCF[16] or Acetylene black were also studied. To gain a fundamental understanding of the ORR mechanism of the composite BSCF/carbon catalysts, rotating ring disk electrode (RRDE) measurements have been performed. This technique allows for the quantification of the hydroperoxide produced during the ORR reaction and, therefore, distinguishes between a 2- or 4-electron transfer ORR process. RRDE measurements showed that composite electrodes possess a notably more positive onset potential for the ORR, a significant increase in the kinetic current and a lower hydroperoxide formation compared to BSCF and Acetylene black single electrodes. Different scenarios where BSCF and AB interact in the ORR in a synergistic fashion have been explored and discussed.

RESULTS AND DISCUSSIONS

The influence of carbon addition on the $Ba_{0.5}Sr_{0.5}Co_{0.8}Fe_{0.2}O_{3-\delta}$ (BSCF) activity and selectivity toward the oxygen reduction reaction (ORR) has been investigated by systematically increasing the carbon (Acetylene black, AB) content in the BSCF electrode, as schematically shown in Figure 1. Table 1 summarizes all the studied electrode compositions. For facilitating the comparison between different electrodes, the overall loading (BSCF, BSCF/AB, AB) was kept constant. For the present study, the used AB carbon was pretreated with concentrated HNO_3. Such acid treatment generally creates carbon−oxygen functional groups on the carbon surface, improving the carbon catalytic activity toward ORR by increasing the availability of oxygen adsorption sites.[4,28−30] XPS spectra of AB before and after the acid treatment (see Supporting Information, Figure S1) showed the formation of

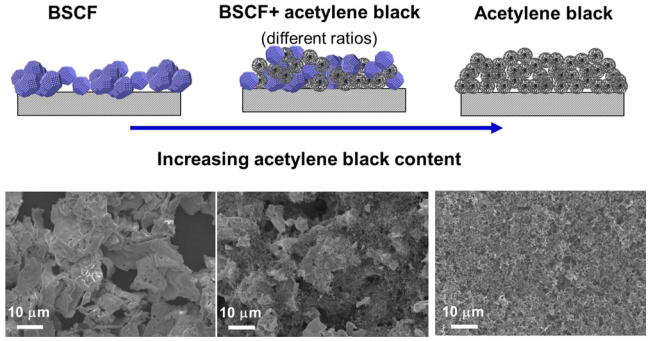

Figure 1. Upper panel: Sketch describing the overall concept of the present work. Lower panel: SEM micrographs of (a) BSCF, (b) BSCF/AB_1.25 and (c) AB electrodes drop-coated and then dried onto glassy carbon substrates.

dx.doi.org/10.1021/cs400903k | ACS Catal. 2014, 4, 1061−1070

Table 1. Electrode Composition (μg cm^{-2}), Weight Ratio between BSCF and AB, and Specific Surface Area (BSCF+AB) Based on the Loading and the BET Surface Area

	BSCF (μg cm^{-2})	AB (μg cm^{-2})	BSCF/AB weight ratio	BSCF+AB specific surface area ($cm^2_{BSCF+AB}$ cm^{-2}_{disk})
BSCF	460	0	1	46
BSCF/AB_10	418	41.8	10	79
BSCF/AB_5	383	76.7	5	107
BSCF/AB_2.5	328.5	131.5	2.5	151
BSCF/AB_1.25	255.5	204.5	1.25	210
BSCF/AB_0.75	179.2	262.8	0.75	254
AB	0	460	0	414

oxygen-containing groups on the carbon surface, such as carboxyl and hydroxyl groups, consistent with literature data.[31,32] In the present case, the treatment in HNO_3 resulted in stabilizing the AB with respect to its ORR activity, allowing reproducible ORR curves (see Supporting Information, Figure S2) to be obtained. The carbon pretreatment maximizes the functional group on its surface and thus its catalytic activity toward the ORR. Differently, the surface of untreated AB can be continuously modified during the polarization curves recorded for the ORR measurement, leading to a variable ORR activity.

Figure 1 shows also the SEM micrographs of a BSCF, BSCF/AB_1.25 and AB electrode after being drop-coated and dried on the glassy carbon substrate. As previously reported,[16] BSCF powder is made of flake-like agglomerates of smaller nanoparticles, with a BET surface area of about 10 m^2 g^{-1}. Due to the morphology and the low surface area of the BSCF powder, completely homogeneous layers could not be achieved, as shown in Figure 1a where the glassy carbon support is still slightly visible. Acid treated AB had a BET surface of about 90 m^2 g^{-1} and formed a homogeneous porous thin layer on the glassy carbon substrate (Figure 1c). The mixture of BSCF and AB also resulted in a homogeneous electrode layer (Figure 1b), where the BSCF appeared uniformly encapsulated into the AB matrix.

Figure 2 illustrates the rotating ring disk electrode (RRDE) measurements of BSCF, AB and all the composite electrodes (0.1 M KOH, 5 mV s^{-1}, room temperature, 1600 rpm, cathodic sweeps). To obtain the true ORR currents, the measured data in O_2 atmosphere have been background corrected by the negative-going scan measured in Ar atmosphere under otherwise identical conditions.[16] For each electrode composition, the corresponding Pt ring current resulting from the oxidation of hydroperoxide species generated at the working electrode is shown in the upper panel. The current plateau in the disk currents characteristic for a diffusion-controlled reaction regime was not observed for any of the electrodes. These results indicate that, for each electrode, the ORR is under a mixed kinetic-diffusion control over the whole potential range. ORR curves of BSCF did not reach either theoretical diffusion limiting current of 5.7 mA cm^{-2} or 2.85 mA cm^{-2} calculated for a 4 or 2 electron process, respectively.[16] On the other hand, the AB electrode reached the theoretical diffusion limiting current for the 2-electron process at the lowest potentials and displayed a two-wave ORR curve, typical for carbon electrodes in alkaline media, which can be explained by the presence of different active surface sites.[4,28,29] Composite electrodes displayed similar two-wave ORR curves, but with less pronounced character. By introducing AB into the BSCF electrode, lower overpotentials for the ORR were achieved (see Figure 2h) with an increased current density at higher overpotentials. Because the overall electrode loading (BSCF +AB μg cm^{-2}) was purposely kept constant, the enhanced performance of the composite electrodes can not be explained by the simple addition of currents resulting from the ORR occurring on the BSCF and the AB surfaces simultaneously.

For a better comparison of the main differences in the ORR activity between the studied electrodes, the onset for the ORR has been arbitrarily defined here as the potential required for an ORR current of -25 μA cm_{disk}^{-2}. As shown in Figure 3a, an optimal BSCF/AB ratio exists and the ORR onset is described by a volcano plot. By introducing only 10 wt % of AB, a significant increase in the onset potential could be already observed. By further increasing the AB content, the ORR onset potential still increased until a maximum value was obtained. The lowest overpotential for the ORR could be achieved for a BSCF and AB weight ratio of 1.25. Upon further increasing the AB content, a slight decrease in the onset for ORR was observed. It is worth highlighting that composite electrodes and in particular the electrode having a BSCF/AB ratio of 1.25 showed ORR onset significantly higher than those of BSCF and AB (about 125 and 70 mV, respectively). Considering the BET surface area of BSCF and AB, the optimal weight ratio corresponds to a surface ratio between BSCF and AB of 0.139, i.e., when the AB surface area is approximately 7 times higher than that of BSCF. A volcano type behavior of the ORR onset as a function of the electrode composition can be also obtained normalizing the ORR currents by the specific surface area (see Table 1), as shown in Figure 3b. In this case, the onset is arbitrarily defined at -2.5 μA $cm_{BSCF+AB}^{-2}$. A maximum is found for the composition having a BSCF to AB weight ratio of 2.5 (about 30 wt % AB), whereas, quite interestingly and possibly by incidence, BSCF and AB show almost the same ORR onset potential on the specific current density scale. Although we do not know the active site neither for BSCF or AB, their number should scale proportionally with the electrode composition. Figure 3b, however, provides striking evidence for enhanced intrinsic catalytic activities within the composite electrodes, maximized in the weight ratio range around 2.5. Possible origins of these enhanced activities in the composite electrodes vs the individual materials will be discussed below.

Apart from the analysis of the ORR onset, a better comprehension of the ORR mechanism can be achieved by the analysis of the Pt ring current. Indeed, the latter allows calculating the hydroperoxide formation at the working electrode and the overall number of electrons transferred during the ORR. From RRDE measurements the mole fraction (in percentage) of hydroperoxide species produced (x_{HO2^-}) and the overall number of transferred electrons (n_{e-}) can be determined by the evaluation of the disk working electrode current (I_d), the ring current (I_r) and its collection efficiency (N) according to following relations:[33]

dx.doi.org/10.1021/cs400903k | ACS Catal. 2014, 4, 1061−1070

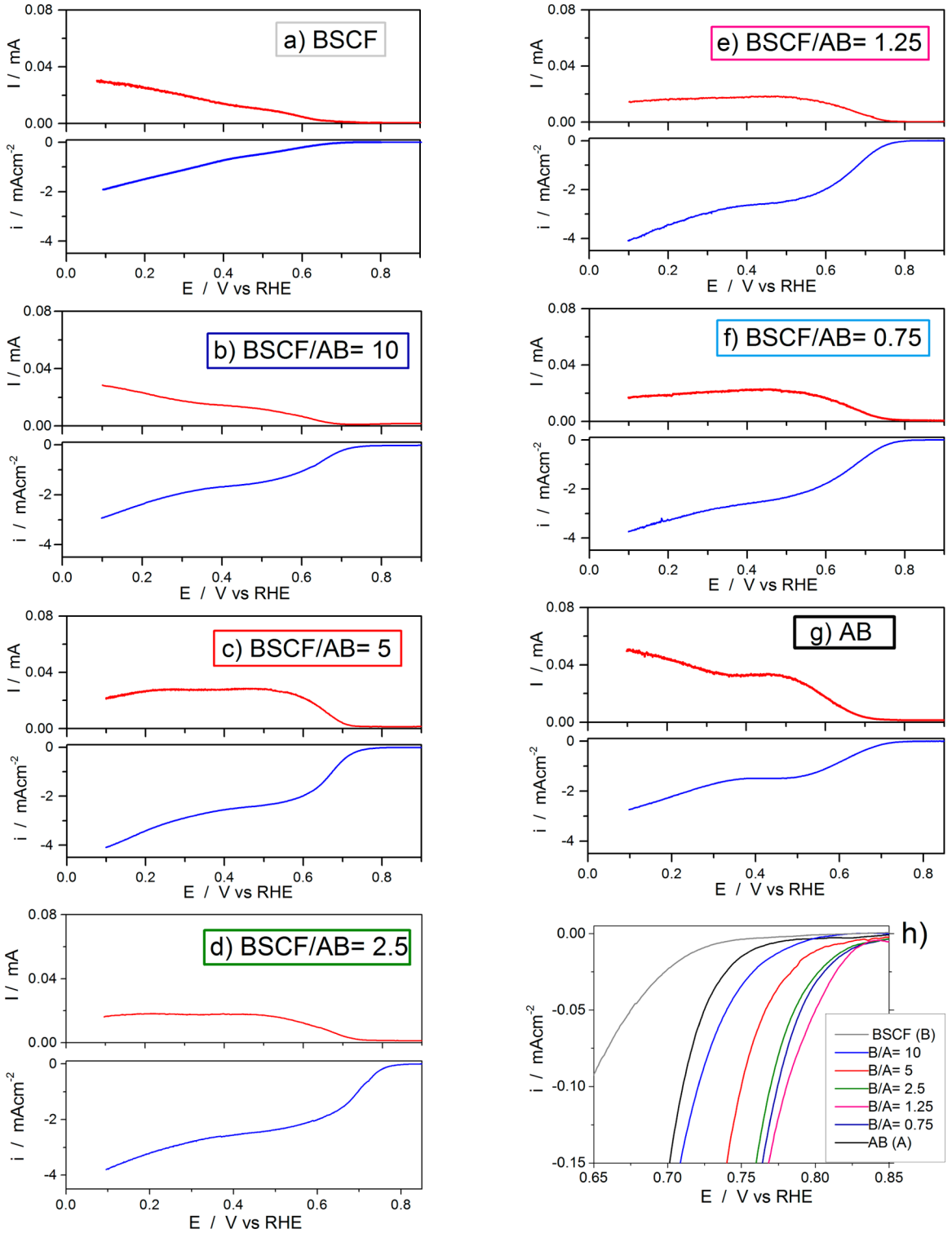

Figure 2. Lower panels: Background corrected ORR currents from cathodic sweeps, 5 mV s^{-1}, 1600 rpm in O_2-saturated 0.1 M KOH. Upper panels: ring currents from the hydroperoxide oxidation, E_{ring} = 1.2 V vs RHE. BSCF (a), BSCF/AB_10 (b), BSCF/AB_5 (c), BSCF/AB_2.5 (d), BSCF/AB_1.25 (e), BSCF/AB_0.75 (f) and AB (g) electrodes (refer to Table 1 for the electrode composition). The ORR currents for the different electrodes in the low overpotential region are also compared (h).

$$x_{HO_2^-}[\%] = 100\frac{2I_r/N}{I_d + I_r/N} \quad (1)$$

$$n_{e^-} = \frac{4I_d}{I_d + I_r/N} \quad (2)$$

The analysis of the RRDE data is summarized in Figure 4, showing the hydroperoxide formation and the overall electrons transferred during the ORR for each tested electrode composition as a function of the applied potential.

As previously reported,[16] for BSCF, the hydroperoxide formation ranges between 50% and 60%. For the acid treated

dx.doi.org/10.1021/cs400903k | ACS Catal. 2014, 4, 1061−1070

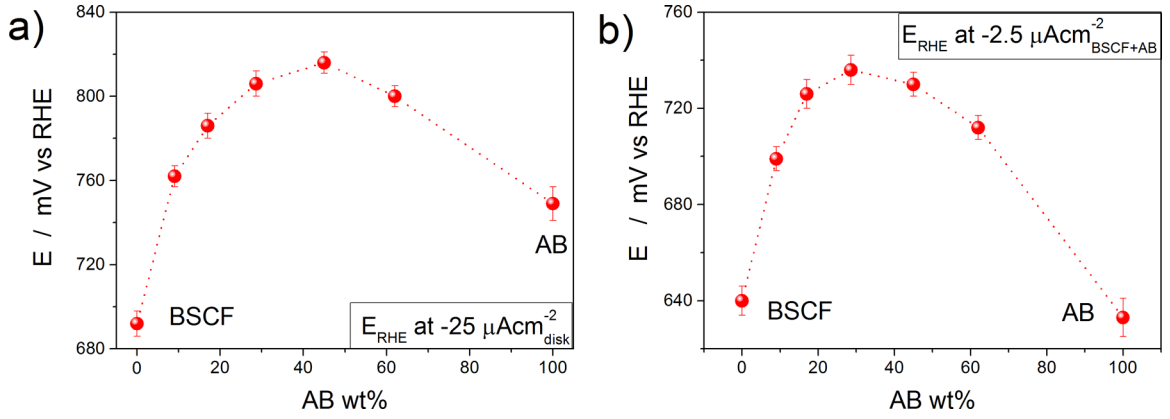

Figure 3. Onset for the ORR (defined as the potential vs RHE reached at −25 μAncm$_{disk}^{-2}$ or at −2.5 μA cm$_{BSCF+AB}^{-2}$) as a function of the AB weight percent in the investigated electrode compositions.

AB, hydroperoxide formation decreased from about 70% to 50% with increased overpotential. Studies on glassy carbon have shown that ORR proceeds mainly via a 2-electron process and only at high overpotentials can oxygen be also partially reduced to water.[34,29] However, on oxidized glassy carbon electrodes, the reduction to OH^- rather than to hydroperoxide is enhanced at all potentials,[34] as observed in the present case for the acid treated AB having surface carbon−oxygen functional groups. Each composite electrode showed lower hydroperoxide formation than both BSCF and AB. Particularly, the hydroperoxide formation was minimized, and thus the number of transferred electrons was maximized, for the sample BSCF/AB_1.25. Figure 4h summarizes the hydroperoxide formation and the number of transferred electrons as a function of the electrode compositions at 0.4 V vs RHE. A volcano type behavior was observed, with a minimum of 28.5% ± 3.5 for the hydroperoxide formation and a maximum of 3.43 ± 0.015 for the number of transferred electrons for the electrode BSCF/AB_1.25. Not surprisingly, this electrode composition also showed the lowest ORR onset overpotential.

As explained above, all the measured ORR curves did not display the current plateau characteristic of diffusion current limitation. Therefore, because the evaluation of the diffusion limiting current from the ORR curves was not possible, we used the number of transferred electrons as determined by RRDE measurements and the following relationship in order to extrapolate the catalyst kinetic currents:

$$\frac{1}{I} = \frac{1}{I_k} + \frac{1}{I_d} = \frac{1}{I_k} + M\frac{1}{n}\cdot\frac{1}{\omega^{1/2}} \quad \text{with } M = 1/\left[0.62FAC_{O_2}(D_{O_2})^{2/3}\upsilon^{-1/6}\right] = const \tag{3}$$

where F is the Faradaic constant, A is the electrode area, C_{O_2} is the oxygen concentration in the electrolyte, D_{O_2} is the oxygen diffusion coefficient, ν is the kinematic viscosity of the electrolyte, and ω is the electrode rotation rate. Using a number of electrons equal to 3, 2.67 and 3.43 for the calculation of I_d for BSCF, AB and BSCF/AB_1.25, respectively, the Tafel plot for these electrodes is reported in Figure 5a. Although no major difference in the Tafel slope was observed (64 mV dec^{-1} for BSCF, 65 mV dec^{-1} for BSCF/AB_1.25, and 55 mV dec^{-1} for AB), the composite electrode showed much improved ORR activity compared to the single BSCF and AB electrode. For example, at 0.725 V vs RHE the kinetic current increased from 0.0053 mA cm^{-2} for the BSCF to 0.0474 mA cm^{-2} for the AB, reaching 0.4965 mA cm^{-2} for the BSCF/AB_1.25. The composite electrode showed, indeed, a kinetic current of 2 and 1 order of magnitude higher than that of BSCF and AB, respectively, and comparable to the kinetic current displayed by other optimized manganese-based ORR catalysts (in the range of 0.1−0.8 mA cm^{-2}).[9] Figure 5 also shows (dotted line) the Tafel plot arising from a simple mathematical combination of the BSCF and AB kinetic currents considering the same BSCF and AB loading as in the BSCF/AB_1.25 composite electrode. The comparison between the latter kinetic current with that measured for the composite electrode shows clearly that a synergistic interaction exists between BSCF and AB. A further evidence is provided by the plot of the potential vs the kinetic current normalized by the catalyst surface area (i_{k,cat_surf}). As shown by Figure 5b, when the ORR kinetic current is normalized by the catalyst specific surface area (see Table 1), BSCF and AB displayed similar activity, while BSCF/AB_1.25 showed kinetic currents more than 1 order of magnitude higher. This result unambiguously shows an enhancement in the catalytic activity toward ORR with respect to single BSCF or AB electrode.

In a first instance, the improvement in performance for the composite electrodes might be ascribed to a relatively limited perovskite electronic conductivity and, thus, to a better electrical connection upon carbon addition. As shown in Figure 1, the BSCF catalyst layer consists of large agglomerates of particles. Addition of carbon would definitively improve the electrical connection between different agglomerates and between the agglomerates and the glassy carbon support. Avoiding that some catalyst agglomerates are not electrically connected, and thus not contributing to the ORR, helps in maximizing the overall surface utilization. Figure 6 illustrates the ORR currents for BSCF (1600 rpm, 5 mV s^{-1}) normalized by the surface area of the oxide (calculated from the loading and the BSCF BET surface area, see also Table 1). Figure 6 also reports the ORR currents normalized by the BSCF surface area but considering a surface area utilization of only 50% and 10% for the ORR. We purposely considered an extreme case where up to 90% of the BSCF surface area is isolated from the conductive support and, hence, would not be contributing to the ORR. Quite evidently, Figure 6 clearly shows that in case

dx.doi.org/10.1021/cs400903k | ACS Catal. 2014, 4, 1061−1070

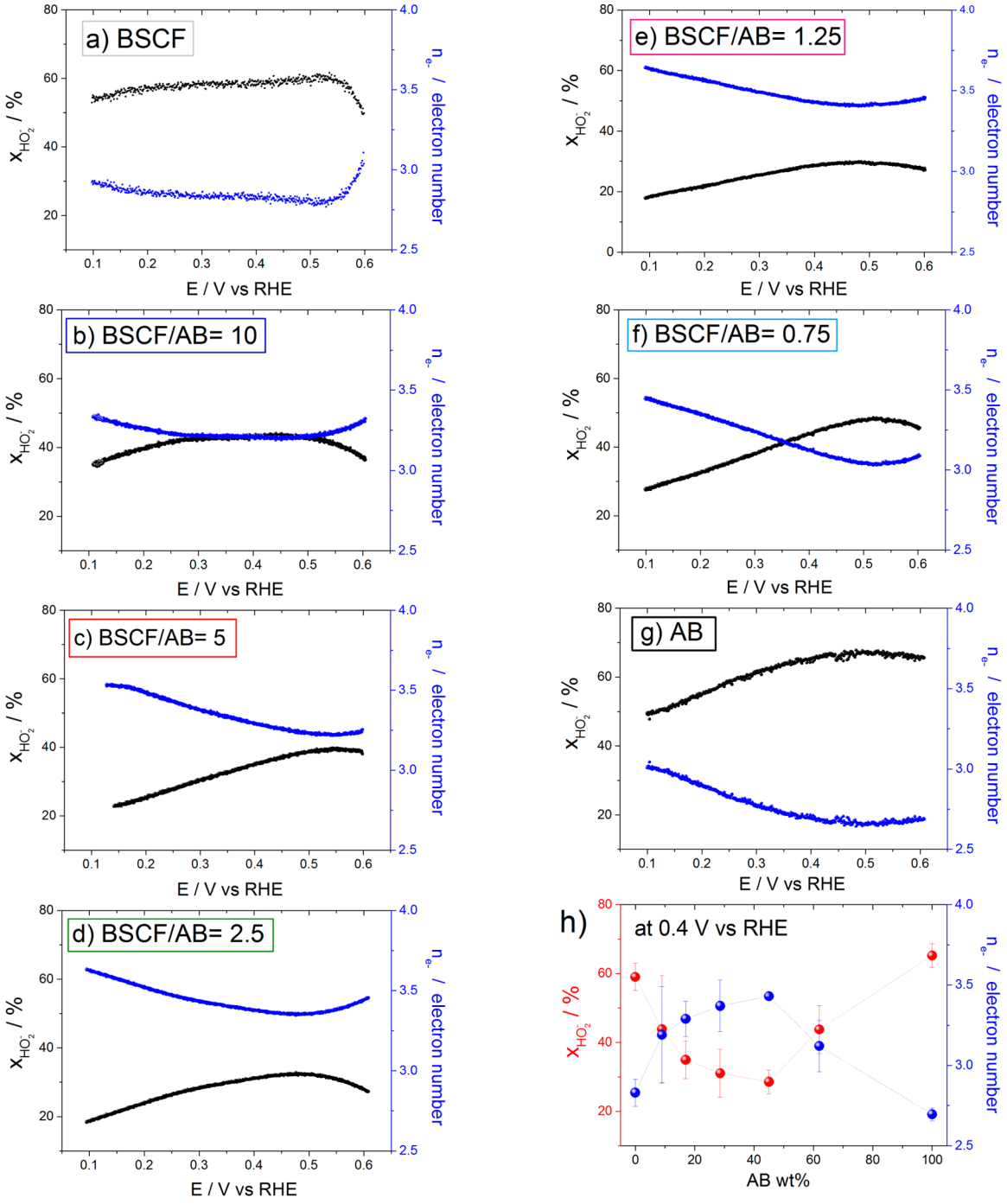

Figure 4. Mole fraction (in percent) of produced hydroperoxide ($x_{HO_2^-}$) and overall number of transferred electrons (n_{e^-}) during ORR as determined by the analysis of the RRDE measurements for the BSCF (a), BSCF/AB_10 (b), BSCF/AB_5 (c), BSCF/AB_2.5 (d), BSCF/AB_1.25 (e), BSCF/AB_0.75 (f) and AB (g) electrodes (refer to Table 1 for the electrode composition). The values for the $x_{HO_2^-}$ and the n_{e^-} calculated at 0.4 V vs RHE are also reported as a function of the AB weight percent (h).

the BSCF powder is poorly electrically connected to the substrate its ORR activity would be underestimated.

Figure 6 also compares the ORR current for the single BSCF electrode, normalized by 100%, 50% and 10% surface utilization, and the ORR current of the BSCF/AB_1.25 composite electrodes, also normalized by the oxide surface area. Even the BSCF ORR currents accounting for only 10% surface utilization showed lower ORR onset than that related to the BSCF/AB_1.25 electrode. Despite being a purely qualitative analysis, this clearly demonstrates that the addition of carbon leads to an additional contribution besides a possible improved BSCF surface utilization. Furthermore, an improvement in BSCF surface utilization would not explain the decrease in hydroperoxide formation for composite electrodes as revealed by the RRDE measurements. Therefore, besides improving BSCF surface utilization, a further interaction must occur between BSCF and AB, involving mechanistic changes in the ORR and leading to superior performance than those of the single electrodes.

dx.doi.org/10.1021/cs400903k | ACS Catal. 2014, 4, 1061−1070

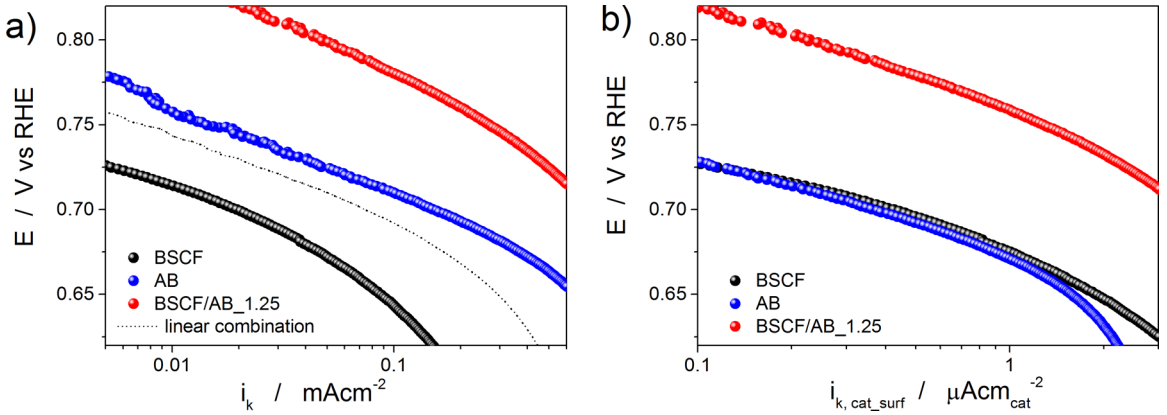

Figure 5. Tafel plot for mass-transport and capacitive current corrected ORR currents obtained from a cathodic scan at 5 mV s^{-1} and 1600 rpm for BSCF, AB and the composite electrode BSCF/AB_1.25. The dotted line represents the polarization curve obtained by the combination of the BSCF and AB experimental kinetic currents considering the same BSCF and AB loading (in wt %) as in the BSCF/AB_1.25 composite electrode (a). Normalization of the Tafel plots by the catalyst specific surface area as reported in Table 1 (b).

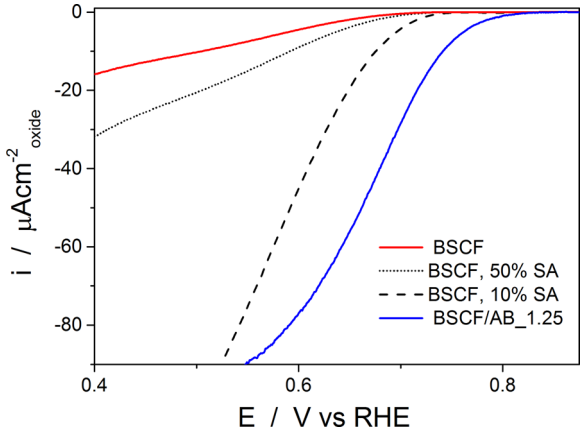

Figure 6. ORR currents for the BSCF and the BSCF/AB_1.25 electrodes measured by cathodically scanning the disk electrode at 5 mV s^{-1} and 1600 rpm in O_2-saturated 0.1 M KOH (currents corrected by the ohmic drop and negative-going scan in Ar atmosphere at 5 mV s^{-1} and 1600 rpm).[16] The currents are normalized by the oxide surface area (SA, calculated from BET surface area and the oxide loading); for the BSCF, ORR currents normalized by only 50% or 10% of the overall SA are also reported.

Depending on the catalyst, the ORR can follow different pathways possibly leading to hydroxide (4-electron process) or hydroperoxide (2-electron process), or to a combination of the two products. Overall, the possible reactions describing the ORR in alkaline environment are summarized in the following (without going into discussions of details of the individual electron and proton transfers):

$$O_2 + 2H_2O + 4e^- \rightarrow 4OH^- \quad (4)$$

$$O_2 + H_2O + 2e^- \rightarrow HO_2^- + OH^- \quad (5)$$

$$HO_2^- + H_2O + 2e^- \rightarrow 3OH^- \quad (6)$$

$$2HO_2^- \rightarrow 2OH^- + O_2 \quad (7)$$

According to reaction 1, a "direct" pathway involving 4-electron transfers occurs describing oxygen reduction to OH^- without forming intermediate HO_2^-. Reaction 2 describes an electrochemical reduction of oxygen where only 2 electrons are involved leading to OH^- and HO_2^- products. The HO_2^- can be then further reduced to OH^- by an additional 2 electrons (reaction 3), or disproportionate chemically, according to reaction 4. In a case where reaction 2 and 3 occur consecutively, the ORR is described to proceed via a "serial" pathway, involving overall 4 electrons. Either the ORR occurring via the "direct" or the "serial pathway" results in high energy-conversion efficiency because overall 4 electrons are transferred. When reaction 4 takes place together with reaction 2, the oxygen produced by the disproportionation of two HO_2^- molecules can be further reduced to OH^- and HO_2^-, leading to an apparent 4-electron ORR mechanism.[9]

In the search of a synergistic effect between BSCF and AB able to explain both the improved ORR activity and the change in hydroperoxide formation, one can assume that the reactions described by reactions 2 and 3 occur on different active sites, i.e., the HO_2^- produced on the AB surface is further reduced to OH^- on the BSCF surface, enhancing the ORR activity and increasing the overall number of transferred electrons. For instance, this would imply fast BSCF kinetics toward hydroperoxide reduction. To evaluate the BSCF activity toward hydroperoxide electroreduction cathodic scans were performed in Ar-saturated 0.1 M KOH + 2×10^{-3} M of HO_2^- electrolyte (similar concentration as C_{O_2} in the ORR). Figure 7 compares the BSCF ORR current and hydroperoxide reduction current at 1600 rpm. The similar shape of the ORR and the hydroperoxide reduction curve suggests that for BSCF the ORR follows the reduction of HO_2^-. Furthermore, the values of the hydroperoxide reduction current are in good agreement with the HO_2^- formation during ORR (about 50%−60%) as revealed by RRDE measurements. As for the ORR, the BSCF hydroperoxide reduction did not reach the diffusion-limiting plateau, suggesting that the latter reaction was under mixed kinetic-diffusion control in the whole potential range and that overall BSCF is not a good catalyst toward hydroperoxide reduction.

Considering the poor catalytic activity of BSCF toward hydroperoxide reduction, it is therefore rather unlikely that the synergistic effect between BSCF and AB consists of a further electrochemical reduction on the BSCF surface of the HO_2^- species produced by the carbon component. However, apart from hydroperoxide electrochemical reduction, BSCF could instead promote hydroperoxide disproportionation, as already reported for other oxide materials. The BSCF activity toward peroxide disproportionation was evaluated by measuring the O_2

dx.doi.org/10.1021/cs400903k | ACS Catal. 2014, 4, 1061−1070

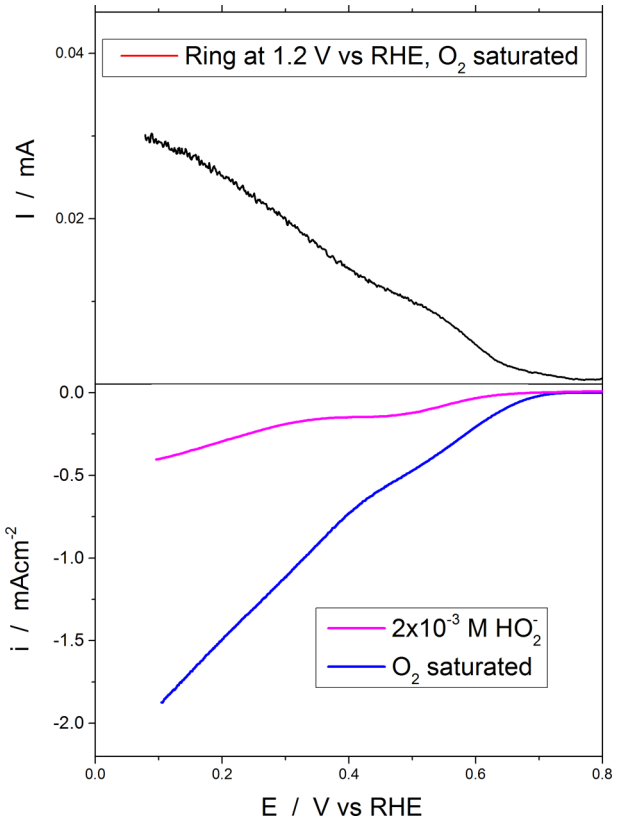

Figure 7. Lower panel: BSCF ORR currents and hydroperoxide reduction currents measured by cathodically scanning the disk electrode at 5 mV s^{-1} and 1600 rpm in O_2-saturated 0.1 M KOH and in Ar-saturated 0.1 M KOH + 2 × 10^{-3} M HO_2^- electrolyte, respectively. Upper panel: ring currents from the hydroperoxide oxidation in O_2 saturated electrolyte, E_{ring} = 1.2 V vs RHE.

concentration with an oxygen sensor as a function of time in 0.1 M KOH containing 2 mM HO_2^- and dispersed BSCF particles. As a reference, the activity of a well-known good catalyst for peroxide decomposition[35−37] (commercial MnO_2 with similar particle size than BSCF) was also measured. Figure 8a shows the increase of O_2 concentration due to spontaneous decomposition of hydroperoxide (no catalyst present, baseline), as well as when the electrolyte solution contained ∼7 mg of BSCF or MnO_2. The oxygen concentration measured when BSCF was dispersed in the electrolyte was definitively larger than the oxygen background arising from spontaneous hydroperoxide decomposition, but also significantly lower compared to the O_2 concentration recorded in the case MnO_2 was used as catalyst. The rate constant for the peroxide decomposition reaction can be calculated plotting $-\ln(1 - [O_2]_t/[O_2]_\infty)$ vs time[37] (where $[O_2]_t$ and $[O_2]_\infty$ represent the oxygen concentration at the time t and $t \rightarrow \infty$, respectively), as shown in Figure 8b. Normalizing the reaction rates for the catalyst mass, for MnO_2 a decomposition capacity of 1.545 ± 0.2 s^{-1} g^{-1}, comparable to other literature data,[37] was obtained. In contrast, BSCF showed a much lower decomposition capacity (0.55 ± 0.25 s^{-1} g^{-1}) compared to MnO_2. These results indicate that even though BSCF displays a certain catalytic activity toward peroxide decomposition, it does not possess high catalytic activity such as, for example, that of MnO_2.

Therefore, analyzing the BSCF catalytic activity toward hydroperoxide electroreduction and decomposition, we could not fully explain the enhancement in ORR catalytic activity and selectivity observed for the composite electrodes assuming a synergistic mechanism where O_2 is first reduced to HO_2^- on AB and then further reduced/decomposed on BSCF. Other synergetic interactions between BSCF and AB should then take place. For example, for composite electrodes made of Co_3O_4-based oxides and N-doped graphene, the formation of a covalent interfacial metal−O−C and metal−N−C bonds were observed by X-ray absorption near edge structure (XANES) measurements.[8,26] Therefore, also in the present case, ligand (electronic) effects between the carbon and the perovskites might lead to a surface electronic tuning of the BSCF by the carbon proximity.

CONCLUSIONS

We have shown that a beneficial interaction between $Ba_{0.5}Sr_{0.5}Co_{0.8}Fe_{0.2}O_{3-\delta}$ (BSCF) perovskite oxide and acid-treated Acetylene black (AB) carbon occurs toward the activity and the selectivity of the oxygen reduction reaction (ORR) in alkaline media. The analysis of different scenarios where BSCF and AB might interact in a synergistic fashion to boost the single electrode ORR activity showed that (1) AB addition can result in an improved BSCF surface utilization, and therefore in

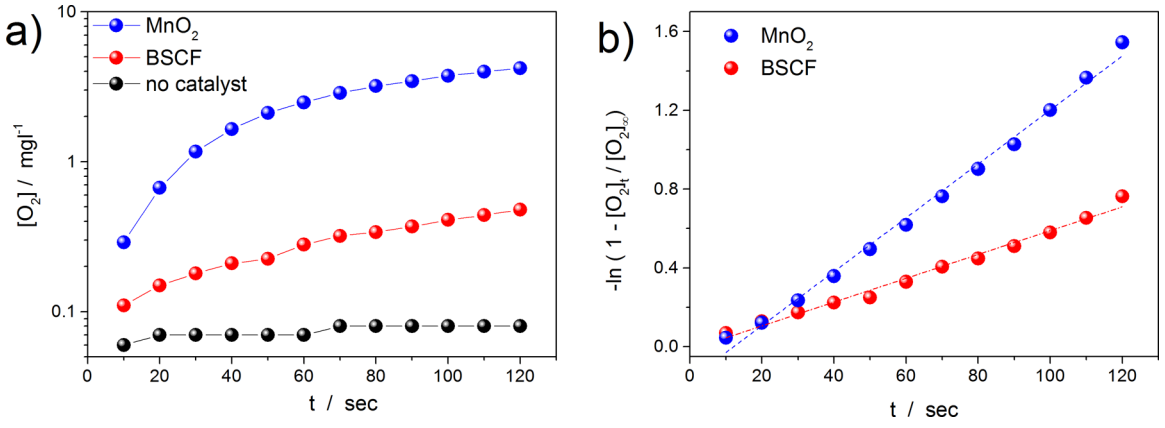

Figure 8. Oxygen concentration as a function of time measured by an oxygen sensor in 0.1 M KOH containing 2 mM HO_2^- and also ∼7 mg of BSCF or commercial MnO_2 powders (a); plot of $-\ln(1 - [O_2]_t/[O_2]_\infty)$ vs time for BSCF and MnO_2 for the evaluation of peroxide decomposition rate constant (b).

dx.doi.org/10.1021/cs400903k | ACS Catal. 2014, 4, 1061−1070

higher ORR currents. However, the latter cannot fully explain the higher activity and selectivity of the composite electrodes compared to single BSCF and AB electrodes. (2) The BSCF activity toward hydroperoxide electroreduction/disproportionation resulted relatively poor to explain a possible synergistic ORR process where oxygen is first reduced on AB to HO_2^-, and then the latter is further reduced/decomposed by the BSCF.

Therefore, other synergistic effects should play a part in the composite electrode ORR process. Hypothetically, BSCF, having a high surface concentration of oxygen vacancies, might easily adsorb oxygen molecules on its surface and the carbon acts as a source of electrons for the ORR. A similar synergy was shown for different oxide/carbon catalyst systems where X-ray absorption near edge structure (XANES) measurements revealed the formation of a surface electronic interaction between the oxide and the carbon, leading to superior ORR catalytic activity by improving the oxide conductivity and catalytic activity.[8,26] Even though a careful investigation of the BSCF and AB electronic structure, when they are coupled together, is out of the scope of this work, the present results highlight the importance of considering BSCF and AB as a composite electrode where the two components operate in a synergetic fashion. Furthermore, the present results open future prospects to improve the ORR activity of perovskite/carbon system such as, for example, improving the surface interaction between the perovskite and the carbon phase. This may lead to a further reduction of the ORR overpotential and of the produced amount of hydroperoxide which is at this stage still too high for practical applications. Certainly, the catalytic activity and selectivity toward ORR of the present composite electrode should be still optimized, particularly if compared to those of Pt-based catalysts. However, it should be also considered that perovskite based-oxides are far cheaper than platinum and, therefore, their loading is limited only by electrode thickness constrains. This means that the lower specific activity can be compensated by a larger mass loading.

EXPERIMENTAL METHODS

$Ba_{0.5}Sr_{0.5}Co_{0.8}Fe_{0.2}O_{3-\delta}$ (BSCF) powders were synthesized using a modified sol−gel process. Stoichiometric quantities of commercial $Ba(NO_3)_2$ (Aldrich, 99%), $Sr(NO_3)_2$ (Aldrich, 99%), $Co(NO_3)_2{\cdot}6H_2O$ (Aldrich, 99%) and $Fe(NO_3)_3{\cdot}9H_2O$ (Aldrich, 98%) nitrate precursors were dissolved in an aqueous solution of 0.2 M nitric acid. Citric acid (Aldrich, 99.5%) was used as a chelating agent in a 2:1 ratio with respect to the total metal cations. After a transparent solution was obtained, the pH was then adjusted between 6 and 8 by NH_4OH additions. The solution was then heated under stirring to evaporate water until it changed into a viscous gel and finally ignited to a flame, resulting in a black ash. To obtain single phase material, the BSCF powder was calcined at 1000 °C for 2 h in air. Phase identification of BSCF powders was carried out using X-ray diffraction (using X-ray diffraction (XRD, Bruker D8 system) with Cu Kα radiation (λ = 0.154 18 nm) in Bragg−Brentano geometry. The specific surface area of the powder, determined by Brunauer−Emmett−Teller (BET) analysis, was about 10 ± 1 $m^2\ g^{-1}$. Acetylene black was purchased from Alfa Aesar and, prior to utilization, it was treated in concentrated nitric acid overnight at 80 °C, then washed and dried at 100 °C. The specific surface area of the acid treated AB was determined by BET and was found to be 90 ± 4 $m^2\ g^{-1}$. For the electrochemical characterization, porous thin films were prepared by drop-coating a cathode ink on a rotating glassy carbon disk.[38] Prior the cathode ink preparation, BSCF powder was slightly grinded in order to reduce the larger powder agglomerates and improve the homogeneity of the ink; the BET surface was not significantly modified compared to the as-prepared powder. The cathode inks were prepared from a suspension made of 15 mg of BSCF/BSCF plus AB/AB, 20 μL of Na^+-exchanged Nafion solution (Nafion 117, Alfa Aesar) and 5 mL of isopropyl alcohol. The catalysts inks were sonicated for 30 min and then an aliquot of 30 μL of catalyst suspension was pipetted on a rotating mirror polished glassy carbon electrode (0.196 cm^2). The total loading was therefore kept constant among all the investigated electrode, being ∼460 $\mu g\ cm^{-2}$ of BSCF/BSCF plus AB/AB and ∼50 $\mu g\ cm^{-2}$ Na^+-exchanged Nafion. The catalyst layer microstructure was observed using a scanning electron microscope (SEM, Gemini Ultra 55). The working electrodes were immersed under potential control (0.8 V vs RHE) in 0.1 M KOH electrolyte saturated with pure Ar or O_2 at room temperature and the measurements were performed using a hydrogen reference electrode (RHE) and a gold counter electrode in a three-electrode configuration. The 0.1 M KOH electrolyte was prepared from Milli-Q water and KOH pellets (Sigma Aldrich, 99.99%). Rotating ring disk electrode (RRDE) measurements were performed in a homemade Teflon cell by cathodically scanning the disk electrode between 1 and 0.05 V at 5 mV s^{-1} while the Pt ring electrode was held at 1.2 V (RHE). Unless otherwise indicated, current densities were normalized to the geometric area of the glassy carbon substrate and all the potentials were corrected by the ohmic drop in the electrolyte measured by electrochemical impedance spectroscopy. Furthermore, the cathodic scan obtained from RRDE measurements of the disk electrodes were also corrected for capacitive currents measured under cathodic scan at 5 mV s^{-1} in Ar-saturated electrolyte.[16] The hydroperoxide formation presented in the paper results from averaging of 3 to 5 independent measurements. The collection efficiency of the Pt ring was 0.2 ± 0.02 and was determined according to ref 39. BSCF hydroperoxide reduction activity was measured by cathodically scanning the disk electrode at 5 mV s^{-1} and 1600 rpm in Ar-saturated 0.1 M KOH + 2 × 10^{-3} M HO_2^- electrolyte. The catalytic activity of BSCF and commercial MnO_2 (Aldrich) toward hydrogen peroxide decomposition was estimated by dispersing under stirring at 100 rpm ∼7 mg of BSCF or MnO_2 into 40 mL of 0.1 M KOH containing 2 mM HO_2^-. The oxygen concentration was measured every 10 s with a commercial oxygen sensor (835A, ThermoOrion). Prior to the addition of the oxide powders, the KOH solution was deaerated by bubbling pure Ar gas for about 1 h. Baseline for spontaneous peroxide decomposition was recorded measuring the O_2 concentration as a function of time in 40 mL of 0.1 M KOH containing 2 mM HO_2^- but not catalyst powder. All the measurements reported were repeated more than 3 times and error bars are included in the data.

ASSOCIATED CONTENT

Supporting Information

X-ray photoelectron spectroscopy (XPS) spectra for the Acetylene black before and after the acid treatment (Figure S1), ORR currents measured by scanning the disk electrode at 5 mV s^{-1} and 1600 rpm in O_2-saturated 0.1 M KOH for the Acetylene black before and after the acid treatment (Figure S2).

dx.doi.org/10.1021/cs400903k | ACS Catal. 2014, 4, 1061−1070

This material is available free of charge via the Internet at http://pubs.acs.org.

AUTHOR INFORMATION

Corresponding Author

*E. Fabbri. E-mail: emiliana.fabbri@psi.ch.

Notes

The authors declare no competing financial interest.

ACKNOWLEDGMENTS

E.F. gratefully acknowledges the Swiss National Foundation (SNF) within the Ambizione project for financial support. R.M., P.L. and O.C. thank the South African Department of Science and Technology for financial support in the form of HySA/Catalysis Centre of Competence programme funding (O.C. and P.L.) and a HySA/Catalysis student bursary (R.M.).

REFERENCES

(1) Gulzow, E. *J Power Sources* **1996**, *61* (1−2), 99−104.
(2) Varcoe, J. R.; Slade, R. C. T. *Electrochem. Commun.* **2006**, *8* (5), 839−843.
(3) Ramaswamy, N.; Mukerjee, S. *J. Phys. Chem. C* **2011**, *115* (36), 18015−18026.
(4) Song, C.; Zhang, J. In *PEM Fuel Cell Electrocatalysts and Catalyst Layers: Fundamentals and Applications*; Zhang, J., Ed; Springer: New York, 2008; pp 89−134.
(5) Schmidt, T. J.; Stamenkovic, V.; Arenz, M.; Markovic, N. M.; Ross, P. N. *Electrochim. Acta* **2002**, *47* (22−23), 3765−3776.
(6) Song, C. J.; Zhang, L.; Zhang, J. J. *J. Electroanal. Chem.* **2006**, *587* (2), 293−298.
(7) Lima, F. H. B.; Calegaro, M. L.; Ticianelli, E. A. *J. Electroanal. Chem.* **2006**, *590* (2), 152−160.
(8) Liang, Y. Y.; Li, Y. G.; Wang, H. L.; Zhou, J. G.; Wang, J.; Regier, T.; Dai, H. J. *Nat. Mater.* **2011**, *10* (10), 780−786.
(9) Gorlin, Y.; Chung, C. J.; Nordlund, D.; Clemens, B. M.; Jaramillo, T. F. *ACS Catal.* **2012**, *2* (12), 2687−2694.
(10) Meadowcr, D. b. *Nature* **1970**, *226* (5248), 847−&.
(11) Morin, F. J.; Wolfram, T. *Phys. Rev. Lett.* **1973**, *30* (24), 1214−1217.
(12) Matsumoto, Y.; Yoneyama, H.; Tamura, H. *J. Electroanal. Chem.* **1977**, *79* (2), 319−326.
(13) Matsumoto, Y.; Yoneyama, H.; Tamura, H. *J. Electroanal. Chem.* **1977**, *83* (2), 237−243.
(14) Suntivich, J.; Gasteiger, H. A.; Yabuuchi, N.; Nakanishi, H.; Goodenough, J. B.; Shao-Horn, Y. *Nat. Chem.* **2011**, *3* (8), 647−647.
(15) Suntivich, J.; May, K. J.; Gasteiger, H. A.; Goodenough, J. B.; Shao-Horn, Y. *Science* **2011**, *334* (6061), 1383−1385.
(16) Fabbri, E.; Mohamed, R.; Levecque, P.; Conrad, O.; Kötz, R.; Schmidt, T. J. *ChemElectroChem* **2013**, DOI: 10.1002/celc.201300157.
(17) Cheriti, M.; Kahoul, A. *Mater. Res. Bull.* **2012**, *47* (1), 135−141.
(18) Yuasa, M.; Yamazoe, N.; Shimanoe, K. *J. Electrochem. Soc.* **2011**, *158* (4), A411−A416.
(19) Jin, C.; Cao, X.; Lu, F.; Yang, Z.; Yang, R. *Int. J. Hydrogen Energ* **2013**, *38* (25), 10389−10393.
(20) Sunarso, J.; Torriero, A. A. J.; Zhou, W.; Howlett, P. C.; Forsyth, M. *J. Phys. Chem. C* **2012**, *116* (49), 26108−26108.
(21) Azizi, F.; Kahoul, A.; Azizi, A. *J. Alloys Compd.* **2009**, *484* (1−2), 555−560.
(22) Li, X. X.; Qu, W.; Zhang, J. J.; Wang, H. J. *J. Electrochem. Soc.* **2011**, *158* (5), A597−A604.
(23) Poux, T.; Napolskiy, F. S.; Dintzer, T.; Kerangueven, G.; Istomin, S. Y.; Tsirlina, G. A.; Antipov, E. V.; Savinova, E. R. *Catal. Today* **2012**, *189* (1), 83−92.
(24) Hardin, W. G.; Slanac, D. A.; Wang, X.; Dai, S.; Johnston, K. P.; Stevenson, K. J. *J. Phys. Chem. Lett.* **2013**, *4* (8), 1254−1259.
(25) Tulloch, J.; Donne, S. W. *J. Power Sources* **2009**, *188* (2), 359−366.
(26) Liang, Y. Y.; Wang, H. L.; Zhou, J. G.; Li, Y. G.; Wang, J.; Regier, T.; Dai, H. J. *J. Am. Chem. Soc.* **2012**, *134* (7), 3517−3523.
(27) Malkhandi, S.; Trinh, P.; Manohar, A. K.; Jayachandrababu, K. C.; Kindler, A.; Surya Prakash, G. K.; Narayanan, S. R. *J. Electrochem. Soc.* **2013**, *160*, F943−F952.
(28) Vaik, K.; Schiffrin, D. J.; Tammeveski, K. *Electrochem. Commun.* **2004**, *6* (1), 1−5.
(29) Tammeveski, K.; Kontturi, K.; Nichols, R. J.; Potter, R. J.; Schiffrin, D. J. *J. Electroanal. Chem.* **2001**, *515* (1−2), 101−112.
(30) Xu, J.; Huang, W. H.; McCreery, R. L. *J. Electroanal. Chem.* **1996**, *410* (2), 235−242.
(31) Biniak, S.; Szymanski, G.; Siedlewski, J.; Swiatkowski, A. *Carbon* **1997**, *35* (12), 1799−1810.
(32) Sullivan, M. G.; Schnyder, B.; Bartsch, M.; Alliata, D.; Barbero, C.; Imhof, R.; Kotz, R. *J. Electrochem. Soc.* **2000**, *147* (7), 2636−2643.
(33) Schmidt, T. J.; Stamenkovic, V.; Ross, P. N.; Markovic, N. M. *Phys. Chem. Chem. Phys.* **2003**, *5* (2), 400−406.
(34) Taylor, R. J.; Humffray, A. A. *J. Electroanal. Chem.* **1975**, *64* (1), 63−84.
(35) Mooi, J.; Selwood, P. W. *J. Am. Chem. Soc.* **1952**, *74* (7), 1750−1754.
(36) Hasan, M. A.; Zaki, M. I.; Pasupulety, L.; Kumari, K. *Appl. Catal., A* **1999**, *181* (1), 171−179.
(37) Mao, L. Q.; Sotomura, T.; Nakatsu, K.; Koshiba, N.; Zhang, D.; Ohsaka, T. *J. Electrochem. Soc.* **2002**, *149* (4), A504−A507.
(38) Schmidt, T. J.; Gasteiger, H. A.; Stab, G. D.; Urban, P. M.; Kolb, D. M.; Behm, R. J. *J. Electrochem. Soc.* **1998**, *145* (7), 2354−2358.
(39) Paulus, U. A.; Schmidt, T. J.; Gasteiger, H. A.; Behm, R. J. *J. Electroanal. Chem.* **2001**, *495* (2), 134−145.